Preprints of the
9th International Symposium on Advanced Control of Chemical Processes
The International Federation of Automatic Control
June 7-10, 2015, Whistler, British Columbia, Canada

Experimental Validation of Robust Process Design and Control Based on Gaussian Mixture Densities ⋆

N. Rossner * **R. King** **

* *Present address: Bayer Technology Services GmbH, Process Dynamics and Operation, Kaiser-Wilhelm-Allee 60, 51368 Leverkusen, Germany (e-mail: niko.rossner@bayer.com).*
** *Berlin Institute of Technology, Department of Measurement and Control, Hardenbergstrasse 62a, 10623 Berlin, Germany (e-mail: rudibert.king@tu-berlin.de).*

Abstract: In this contribution, the effects of different degrees of uncertainty description are investigated experimentally using an exothermic chemical reaction with safety constraint on the temperature. For that purpose, two robust trajectories are designed that respect the artificially created uncertainties of the experiments either coarsely using a single multivariate normal distribution (1GMD) or in a more detailed fashion using a Gaussian mixture density (GMD) consisting of 32 multivariate normal densities (32GMD). For the optimization, the uncertainties are propagated using the unscented transformation. Both trajectories were run 71 times in an open-loop manner. The more detailed trajectory (32GMD) leads to a 9 % higher yield without increasing the risk of constraint violation. Furthermore, many experimental realizations of two robust closed-loop process control schemes are being compared. They differ again only in the degree of the underlying uncertainty description. Although the frequent corrections of the controller marginalize the advantage of a more detailed stochastic process prediction, the 4GMD-controller still allows for 3 % more educt conversion compared to the 1GMD-controller.

Keywords: Uncertain Dynamic Systems, Nonlinear Systems, Gaussian Distributions, Probabilistic Simulation, Reactor Control, Safety-Critical, Robust control, Validation

1. INTRODUCTION

Technical processes are influenced by a variety of uncertain input and model parameters. The variation of these values often has a significant impact on the development a process. The specific process behavior is especially important when safety constraints come into play. While the exact values of the uncertain parameters are not known, their probabilistic description is often available. In most cases, normal densities are used to reflect the uncertain parameters. In order to obtain a prediction of the uncertainties, the normal densities have to be propagated through the nonlinear model equations. A numerically efficient stochastic simulation is the *Unscented Transformation* (UT) presented by *Julier* and *Uhlmann*. It represents each uncertain parameter by its mean value and two so-called sigma-points. The statistical moments of the output are calculated by solving the model equations for the mean vector as well as for all sigma-points and applying an explicit formula on these solutions. It thus corresponds to a gradient-free approximation of 2^{nd} order [Julier and Uhlmann (1996); Julier et al. (2000); Nørgaard et al. (2000); van der Merwe (2004)].

The method is limited, however, in that the process variables are only represented as normally distributed, and, thus, being symmetrically uncertain. In nonlinear systems, however, normally distributed inputs will inevitably lead to distorted, asymmetrical probability densities. In order to describe arbitrary process input densities, and to better account for effects in nonlinear density propagation a Gaussian mixture density (GMD) can be used [Rossner et al. (2010)]. As here each individual density has a lower variance, nonlinear deforming effects will be less pronounced during propagation. A linear combination of normal densities can be simulated by superposition of the *Unscented Transformations* of the individual densities. This method has been proposed before [Rossner et al. (2010)] to design robust processes. Results, as with other methods, have been presented so far only with simulation studies. Hence, the primary goal of this work is to give an experimental validation.

In this contribution, the impact of different degrees of uncertainty description, single multivariate normal density and Gaussian mixture density, on open- and closed-loop process control is investigated experimentally. For that purpose a fully-automated semibatch reactor for the catalytic decomposition of hydrogen peroxide H_2O_2 is set up. Defined disturbances on the initial amount of catalyst V_0 and the cooling temperature T_M are introduced to the individual process runs. Over all process runs these disturbance samples are normally distributed. Moreover, an upper safety-constraint on the reactor temperature is introduced. This limits the production rate of the exothermic process and the process result, thus, highly depends on the prediction of the probability density along that constraint. If an overestimation of its variance can be avoided, the production capabilities can be better exploited and more yield can be expected.

In the first part of this contribution, the fully-automated chemical reactor is presented and the underlying mathematical model is introduced. Subsequently, the experimental results of both robust open-loop process designs (TP), 1GMD-TP and 32GMD-

⋆ A version in German language of this contribution has been presented in "at Automatisierungstechnik 68, Issue 1, 2014, Page 14-22".

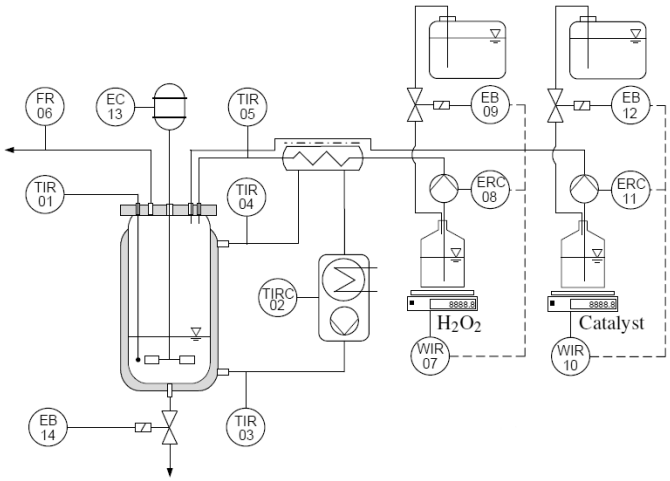

Fig. 1. P&I-Diagram of the automated reaction system. **01:** Reactor temperature. **02:** Thermostat temperature. **03:** Cooling temperature, supply. **04:** Cooling temperature, return. **05:** Feed Temperature. **06:** O_2 volume flow. **07:** Weight of buffer tank, H_2O_2. **08:** Voltage for dosing pump, Feed. **09:** Magnetic valve to storage tank of educt. **10:** Weight of buffer tank, catalyst. **11:** Voltage for dosing pump, catalyst. **12:** Magnetic valve to storage tank of catalyst. **13:** Motor voltage for stirrer. **14:** Magnetic valve to dump vessel.

TP, are shown. The more detailed prediction of process uncertainties using 32 normal densities leads to a 9 % higher productivity compared to the 1GMD design. Hereafter, online-optimization is introduced, and, thus, the results of the closed-loop process designs are presented. Due to the frequent corrections of the controller uncertainties have less impact on the process result. However, the control design based on the more detailed uncertainty description still leads to a 3 % higher yield compared to the one based on a single normal distribution. The contribution finally ends with a brief discussion of the obtained results.

2. EXPERIMENTAL SETUP

In order to run a large number of specifically disturbed processes with a high repeatability a fully-automated reactor system has been set up. This allows for running the semibatch reaction all around the clock, and, thus, enables the realization of all process runs in a timely manner. For each disturbance sample, the different control designs are run in an alternating fashion to ensure that remaining non-modeled disturbances affect both designs similarly.

Fig. 1 shows the experimental setup with all sensors and actuators using a piping and instrumentation (P&I) diagram. The jacket-cooled reactor has a diameter of $d = 0.1\,\mathrm{m}$ and holds a maximum of 2 L. When a process is initiated the disturbance samples for the initial volume of catalyst V_0 and the cooling temperature T_M are read from the database. In order to ensure an isoperibolic [1] process campaign, the cooling temperature T_M is send to the thermostat (02) and the initial volume V_0 is used as set-point for a pump-scale-controller of the catalyst. The dosage of the catalyst is realized with a tolerance of 0.1 g. In order to reach the starting reactor temperature $T(t_0) = T_\mathrm{M}$ more quickly, the stirrer (13) is activated with the dosage of the catalyst. Moreover, before the catalyst enters the reactor it is pre-cooled or -heated by a heat exchanger embedded in the reactor cooling circuit. This heat exchanger is also used to ensure a defined feed temperature $T_\mathrm{feed} = T_\mathrm{M}$. Once the temperature of the catalyst has reached the cooling temperature with a tolerance of $\Delta T_0 = 0.5\,\mathrm{K}$ the process is initiated. Now, the sensor signals are being written to the database using the sample interval Δt_meas. At the same time, the feeding profile q_f of the specific process run is read from the database and transferred to the feed-controller (07, 08) using a zero-order-hold scheme. The stirrer is used to homogenize the reaction mixture, to improve the heat transfer to the cooling jacket, and to avoid an over-saturation of dissolved oxygen for a more direct measurement of its evolution rate (06) during the model identification experiments (not shown). Once the end of the process t_end is reached, the reaction will be cooled down to the exit temperature T_ab and then released via the magnetic relief valve (14). The weight controlled buffer tanks for educt H_2O_2 and the catalyst are automatically refilled by opening the valves (9,12) to the tanks. Because the tanks are positioned higher than the buffer vessels this procedure is driven by hydrostatic pressure. A new process cycle is initiated as soon as the control system is connected to the next prepared database.

[1] The disturbance is constant during each process run. Over all runs these values are normally distributed.

3. PROCESS MODEL

The chemical decomposition of hydrogen peroxide (H_2O_2, Index 'hp') involves at least four substances. Due to the presence of potassium iodine (PI) the educt H_2O_2 will be catalytically decomposed into the products $H_2O^{(l)}$ (Index 'w') and $O_2^{(g)}$ (Index 'o'). Oxygen leaves the reactor as exhaust gas. The exothermic reaction has reaction rate r and reaction enthalpy ($-\Delta H_\mathrm{R}$). It can thus be written as:

$$\mathrm{H_2O_2} \xrightarrow[r]{\mathrm{PI}} \mathrm{H_2O} + \frac{1}{2}\mathrm{O_2} + (-\Delta H_\mathrm{R})\,. \tag{1}$$

In this reaction scheme, PI is modeled as a perfect catalyst that is not being consumed. This is a slight simplification compared to the more complex reaction scheme of the Bray-Liebhafsky reaction [Bray and Liebhafsky (1931); Liebhafsky and Mohammad (1933); Schmitz (2011)] which also involves other substances, e.g., the formulation of Iodine I_2. The reaction enthalpy in (1) is approximately $(-\Delta H_\mathrm{R}) = 100.4$ kJ/mol (Steudel et al. (2008)). Since both educt and catalyst concentration influence the reaction rate r, the rate has been modeled as a reaction of second order:

$$r = k_0\, e^{\frac{-E_\mathrm{A}}{RT}}\, c_\mathrm{hp}\, c_\mathrm{PI} \qquad \left[\frac{\mathrm{mol}}{\mathrm{L\,s}}\right]. \tag{2}$$

Here, c_hp and c_PI are the molar concentrations of hydrogen peroxide and potassium iodine, respectively. The constants $k_0 \approx 10^9$ L/mol/s and $E_\mathrm{A} \approx 54$ kJ/mol (Liebhafsky and Mohammad (1933)) represent the rate factor and the activation energy, respectively, and allow for the temperature depending description of the reaction rate according to *Arrhenius*. The factor k_0, however, will still be treated as a free parameter in order to create a degree of freedom for the model identification based on the obtained data.

Mole Balance

Based on the description of the reaction rate r the amounts of the reactants can be balanced. In a semibatch process the rate of the amount n_i, $\dot{n}_i$, of substance i depends on the reacting amounts $\dot{n}_{\mathrm{R},i}$ as well as the feeding $\dot{n}_{\mathrm{f},i}$:

$$\begin{aligned}\dot{n}_i &= \dot{n}_{\mathrm{R},i} + \dot{n}_{\mathrm{f},i} \\ &= \nu_i\, r V + \frac{1}{M_i}\,\rho_i\, q_{\mathrm{f},i}\,. \end{aligned} \tag{3}$$

Each reactant i has the molar mass M_i, density ρ_i and is being fed according to $q_{\mathrm{f},i}$. Based on the stochiometry in (1) the following stochiometric coefficients ν_i can be derived:

$$\nu_{\mathrm{hp}} = -1 \quad \nu_{\mathrm{w}} = +1 \quad \nu_{\mathrm{PI}} = 0 \quad \nu_{\mathrm{o}} = +\frac{1}{2}. \tag{4}$$

Out of the four considered substances only H_2O_2 (hp), H_2O (w) und PI are balanced as system states as they contribute to the reaction mass. Oxygen on the other hand leaves the system right away and is therefore not considered as system state. Its evolution rate $\dot{n}_{\mathrm{o}} = 1/2\, rV$, however, is contributing to the heat balance later on. The reaction volume is calculated at every time point from the amounts of hydrogen peroxide n_{hp} and water n_{w}. When neglecting the temperature-dependence of the densities ρ_{hp} and ρ_{w} as well as the potential excess volume of the dissolved PI salt (25 g/L) the reaction volume V can be written as:

$$V \;=\; V_{\mathrm{hp}} + V_{\mathrm{w}} \;=\; \frac{M_{\mathrm{hp}}}{\rho_{\mathrm{hp}}}\, n_{\mathrm{hp}} \;+\; \frac{M_{\mathrm{w}}}{\rho_{\mathrm{w}}}\, n_{\mathrm{w}}. \tag{5}$$

The feed consists of an approximately 30 % watery H_2O_2-solution. By introducing the parameter χ for the uncertain H_2O_2 ratio the average density $\bar{\rho}_{\mathrm{f}}$ of the feed reads:

$$\bar{\rho}_{\mathrm{f}} \;=\; \chi\, \rho_{\mathrm{hp}} + (1-\chi)\, \rho_{\mathrm{w}} \tag{6}$$

Thus, the fed amount of water and hydrogen peroxide, $\dot{n}_{\mathrm{f},i}$ ($i = \mathrm{hp}, \mathrm{w}$) depending on the total feed q_{f} is

$$\dot{n}_{\mathrm{f,hp}} = \frac{\chi}{M_{\mathrm{hp}}}\, \bar{\rho}_{\mathrm{f}}\, q_{\mathrm{f}} \qquad \dot{n}_{\mathrm{f,w}} = \frac{(1-\chi)}{M_{\mathrm{w}}}\, \bar{\rho}_{\mathrm{f}}\, q_{\mathrm{f}}. \tag{7}$$

The total mole-balance of the system states H_2O_2, H_2O, and PI then gives

$$\dot{n}_{\mathrm{hp}} = -\, rV \;+\; \frac{\chi}{M_{\mathrm{hp}}}\, \bar{\rho}_{\mathrm{f}}\, q_{\mathrm{f}} \tag{8}$$

$$\dot{n}_{\mathrm{w}} = +\, rV \;+\; \frac{(1-\chi)}{M_{\mathrm{w}}}\, \bar{\rho}_{\mathrm{f}}\, q_{\mathrm{f}} \tag{9}$$

$$\dot{n}_{\mathrm{PI}} = 0, \tag{10}$$

with reaction rate r, reaction volume V and average feed density $\bar{\rho}_{\mathrm{f}}$ from (2), (5), and (6). Theoretically, the constant amount of catalyst could also be modeled as a parameter. In the given model description, however, all substances that contribute to the reactor mass are considered as system states. Material constants can be found in Tab. 4.

Energy balance

Neglecting the stored heat of the reactor body and equipment parts the heat in the reactor consists of the heat of the individual substances i: $Q_{\mathrm{R}} = \Sigma_i m_i\, c_{p,i}\, T$. Assuming constant specific heat capacities $c_{p,i}$ its time derivative reads:

$$\dot{Q}_{\mathrm{R}} = \frac{\mathrm{d}}{\mathrm{d}t}\Big(\sum_i m_i\, c_{p,i}\, T\Big) = \sum_i \dot{m}_i\, c_{p,i}\, T + \sum_i m_i\, c_{p,i}\, \dot{T} = \sum_k \dot{Q}_k. \tag{11}$$

It is equal to the sum of heat flows $\Sigma_k \dot{Q}_k$ into and out of the system. The heat flows considered in the model are first given mathematically and will be further explained afterwards.

$$\begin{aligned}\sum_k \dot{Q}_k = &\underbrace{\left(\dot{n}_{\mathrm{f,hp}}\, M_{\mathrm{hp}}\, c_{p,\mathrm{hp}} + \dot{n}_{\mathrm{f,w}}\, M_{\mathrm{w}}\, c_{p,\mathrm{w}}\right) T_{\mathrm{f}}}_{\text{Feed}} \\ &+ \underbrace{r V \left(-\Delta H_{\mathrm{R}}\right)}_{\text{Reaction Heat}} - \underbrace{\alpha A\, (T - T_{\mathrm{M}})}_{\text{Jacket Cooling}} \\ &- \underbrace{\dot{n}_{\mathrm{o}}\, M_{\mathrm{o}}\, c_{p,\mathrm{o}}\, T}_{\text{Exhaust Gas}} - \underbrace{\Delta H_{\mathrm{v}}\, \dot{n}_{\mathrm{w}}^{(\mathrm{g})}}_{\text{Vaporization}} \\ &- \underbrace{\dot{n}_{\mathrm{w}}^{(\mathrm{g})}\, M_{\mathrm{w}}\, c_{p,\mathrm{w}}\, T}_{\text{Exhaust Vapor}} - \underbrace{\varepsilon\, \sigma\, A_{\mathrm{rad}}\, (T - T_{\mathrm{M}})^4}_{\text{Radiation}}. \end{aligned} \tag{12}$$

First of all, heat is generated by the exothermic reaction that is characterized by reaction rate r and enthalpy $(-\Delta H_{\mathrm{R}})$. Due to the feed streams $\dot{n}_{\mathrm{f,hp}}$ and $\dot{n}_{\mathrm{f,w}}$ heat is also added depending on the feed temperature T_{f}. The cooling jacket on the other hand removes heat and the resulting heat stream is described by the common phenomenological approach. The surface for this heat transfer A, however, increases linearly with the reaction volume V. Because of foam generation during high reaction rates the heat transfer αA has been modeled with an additional dependence on the reaction rate r. This results in the following characterization of the heat transfer αA in (12) using the parameters a, b and c:

$$\alpha A = aV + b \;+\; c\, r \qquad \left[\frac{\mathrm{J}}{\mathrm{s\,K}}\right]. \tag{13}$$

The strong oxygen evolution during the reaction also results in a significant heat loss. Its temperature is assumed to be equal to the reaction temperature T. Moreover, water evaporates. The resulting heat loss depends on the evaporation enthalpy ΔH_{v} and the exhaust mass flow. The evaporation enthalpy is assumed to be constant using $\Delta H_{\mathrm{v}} = 43$ kJ/mol, which corresponds to a reference temperature of 50C. For the calculation of the exhaust mole flow $\dot{n}_{\mathrm{w}}^{(\mathrm{g})}$ full vapor saturation of the exiting oxygen is assumed. The exhaust stream driven by the vapor pressure p_{w} has been neglected, such that the exhaust stream of water $\dot{n}_{\mathrm{w}}^{(\mathrm{g})}$ is proportional to the oxygen evolution rate: $\dot{n}_{\mathrm{w}}^{(\mathrm{g})} = x_{\mathrm{w}}^{(\mathrm{g})}\, \dot{n}_{\mathrm{o}}$. The vapor fraction $x_{\mathrm{w}}^{(\mathrm{g})} = p_{\mathrm{w}}^{\mathrm{sat}}(T)/p_0$ can be derived from the saturated steam pressure $p_{\mathrm{w}}^{\mathrm{sat}}(T)$ at the current reaction temperature $T = 273.15\,\mathrm{K} + \vartheta$ using Magnus formula [Sonntag (1990)]:

$$p_{\mathrm{w}}^{\mathrm{sat}}(\vartheta) \;=\; p_{\mathrm{w}}^{\mathrm{sat}}(0)\, e^{\frac{17.62\,\vartheta}{243.12\,^{\circ}\mathrm{C} + \vartheta}}, \qquad p_{\mathrm{w}}^{\mathrm{sat}}(0) = 611\,\mathrm{Pa}. \tag{14}$$

Hence, the exhaust mole flow of vapor in (12) is written as

$$\dot{n}_{\mathrm{w}}^{(\mathrm{g})} \;=\; x_{\mathrm{w}}^{(\mathrm{g})}\, \dot{n}_{\mathrm{o}} = \frac{p_{\mathrm{w}}^{\mathrm{sat}}(T)}{p_0}\, \dot{n}_{\mathrm{o}}\,, \tag{15}$$

while the corresponding mass loss has been neglected in the calculation of the reaction volume V.

Finally, heat loss due to radiation shall also be considered. The emissivity of water $\varepsilon = 0.965$, the radiation surface of the reactor $A_{\mathrm{rad}} = 0.05\,\mathrm{m}^2$ [2], the Boltzmann constant $\sigma = 5.67 \cdot 10^{-8}\,\mathrm{W\,m^{-2}\,K^{-4}}$ and the forth power of the temperature difference between reactor and cooling jacket determine the radiated heat loss. It never exceeds 20 mW, which corresponds to only 0.01 K/s. Regarding the roughly 300 s long hot phase of the semibatch, however, it accumulates to temperature difference of about 3 K.

[2] Due to the foam evolution an exact value cannot be calculated. The value is based on an average level of 11 cm.

Based on the formulation of the heat change in the reactor (11) and the above modeled heat streams (12) the change of the reaction temperature can be calculated:

$$\dot{T} = \frac{\overbrace{\sum_k \dot{Q}_k}^{\text{Heat flows}} - \overbrace{\sum_i \dot{m}_i c_{p,i} T}^{\text{Conversion}}}{\underbrace{\sum_i m_i c_{p,i}}_{\text{Heat Capacity}}}, \tag{16}$$

with conversion term $\Sigma_i \dot{m}_i c_{p,i} T$ and absolute heat capacity $\Sigma_i m_i c_{p,i}$ according to:

$$\sum_i \dot{m}_i c_{p,i} T = \left(\dot{n}_{\text{hp}} M_{\text{hp}} c_{p,\text{hp}} + \dot{n}_{\text{w}} M_{\text{w}} c_{p,\text{w}}\right) T \tag{17}$$

$$\sum_i m_i c_{p,i} = n_{\text{hp}} M_{\text{hp}} c_{p,\text{hp}} + n_{\text{w}} M_{\text{w}} c_{p,\text{w}} + n_{\text{PI}} M_{\text{PI}} c_{p,\text{PI}}. \tag{18}$$

The conversion term describes the change of reaction temperatur T based on the mass conversion due to the reaction, and, thus, the change of heat capacity.

Model equations

Defining the system states $\underline{x} = \left(n_{\text{hp}}, n_{\text{w}}, n_{\text{PI}}, T\right)^{\text{T}}$ and the feed rate as manipulating value $u = q_{\text{f}}$, the following nonlinear time-invariant differential equations can be formulated:

$$\dot{\underline{x}} = \begin{pmatrix} \dot{n}_{\text{hp}} \\ \dot{n}_{\text{w}} \\ \dot{n}_{\text{PI}} \\ \dot{T} \end{pmatrix} = \underline{f}(\underline{x}, u, \underline{\theta}) \ . \tag{19}$$

The right hand side $\underline{f}(\underline{x}, u, \underline{\theta})$ represents the terms in (8)-(10) and (16). The only measurement $\underline{y}$ of the semibatch process is the temperature T. Thus, the measurement equation reduces to

$$\underline{y} = T = \underline{h}(\underline{x}). \tag{20}$$

The free model parameters $\underline{\theta} = (k_0, a, b, c, \chi)^{\text{T}}$ have been determined based on 15 identification experiments using the *maximum likelihood estimation* (MLE). The result is given in Tab. 1. Here, the covariance of the temperature has been set to $\mathbf{C}_\eta = 0.35^2\,\text{K}^2$. Beyond the parameter identification its covariance matrix $\mathbf{C}_{\underline{\theta}}$ has been analyzed using 1000 bootstrap simulations [Efron (1986)]. The result is given in Tab. 2.

Parameter Values				
k_0	a	b	c	χ
$0.250 \cdot 10^9$ $\frac{\text{L}}{\text{mol s}}$	12.95 $\frac{\text{J}}{\text{s K m}^3}$	1.470 $\frac{\text{J}}{\text{s K}}$	$7.071 \cdot 10^3$ $\frac{\text{JL}}{\text{mol K}}$	0.270 1

Table 1. Identified parameter vector $\underline{\theta}$ from the non-linear MLE fit based on 15 distinctively disturbed experiments.

4. ROBUST PROCESS DESIGN

Using the dynamic model introduced above defined uncertainties for the initial reaction volume V_0, the jacket cooling temperature T_{M}, and the model parameters are introduced. Considering these uncertainties, two robust process designs, i.e., two open-loop trajectories, with different degrees of uncertainty description are derived from a robust optimization scheme. In both cases, the uncertainties are represented by sigma-points and simulated using the *Unscented Transformation* [Nørgaard et al. (2000)]. Both process designs are then applied to the testing plant multiple times in an alternating manner. The input uncertainties, the initial reaction volume V_0 and the jacket cooling temperature T_{M}, are realized experimentally using deterministic Halton-Samples [Tørvi and Hertzberg (1998)] representing a constant disturbance for each run. This experimental campaign has two goals: The uncertainty prediction of the different degrees of uncertainty description shall be verified, and it shall be demonstrated that a higher degree of uncertainty consideration can be beneficial for the productivity in processes with safety constraints without an increase of risk.

The process inputs T_{M} and V_0 are being disturbed in an uncorrelated manner using a normal distribution. The corresponding standard deviations are chosen to be $\sigma_T = 5\,\text{K}$ for the cooling temperature and $\sigma_V = 15\,\text{mL}$ (5 %) for the initial volume of catalyst. The two robust designs that are being compared are calculated based on a stochastic simulation with a single normal distribution (1GMD) and a more detailed description based on a Gaussian mixture density consisting of 32 normal distributions (32GMD).

While the impact of the uncertain initial volume V_0 is simulated in both cases using a single normal density, the cooling temperature T_{M} is described differently as illustrated in Fig. 2. The 1GMD design applies its normal distribution (upper plot, black line) directly to the simulation. The 32GMD design, however, is using 16 weighted normal densities (gray) to describe the original distribution of the cooling temperature. The corresponding sigma-points of each distribution have the optimal step size $h = \sqrt{3}\sigma$ [Nørgaard et al. (2000)] and are shown as dots on the proprietary density to allow for a better overview. For the 32GMD design the 1000 parameter samples from the bootstrap analysis have been transferred into two multivariate normal densities using the *Expectation Maximization* (EM) algorithm [Dempster et al. (1977)]. Thus, $2 \cdot 16 = 32$ multivariate normal densities are considered for the 32GMD design.

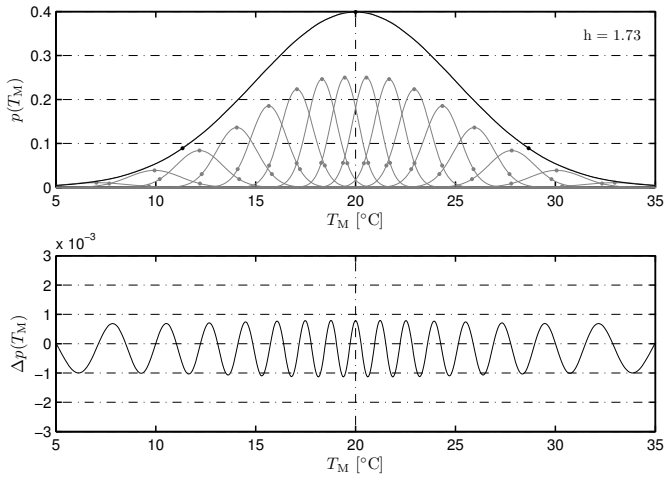

Fig. 2. Description of the uncertain cooling temperature using 1 and 16 normal densities, respectively. Top: Probability densities of the cooling temperature used by the 1GMD design (black) and the 32GMD design (gray). The locations of the sigma-points are shown on the densities themselves. Bottom: Approximation error for the description with 16 normal densities. Within the most relevant $\pm 2\sigma$ area (10-30 °C) the relative error never exceeds 2 %.

	Covariances				
Parameter	k_0	a	b	c	χ
k_0	$0.693 \cdot 10^{9}$	$-0.103 \cdot 10^{3}$	$44.897 \cdot 10^{3}$	$-84.265 \cdot 10^{3}$	-0.316
a		$92.449 \cdot 10^{-6}$	$-41.314 \cdot 10^{-6}$	$8.322 \cdot 10^{-3}$	$31.127 \cdot 10^{-9}$
b			$19.460 \cdot 10^{-6}$	$-6.741 \cdot 10^{-3}$	$-6.221 \cdot 10^{-9}$
c				$0.116 \cdot 10^{3}$	$0.121 \cdot 10^{-3}$
χ					$0.407 \cdot 10^{-9}$

Table 2. Covariance matrix of the parameters $\mathbf{C}_{\underline{\theta}}$ resulting from a bootstrap analysis based on 1000 samples. Only numerical values without their corresponding units.

The process design aims to maximize the amount of product H_2O within the given batch time $t_{\text{end}} = 600\,\text{s}$ without violating the safety constraint on the temperature which was set to $T_{\max} = 345\,\text{K}$. Beyond that, the remaining amount of educt shall be as small as possible. The temperature constraint is implemented in the optimization problem as an inequality condition while the amount of educt at the end of the batch is considered using a penalty term. This results in the following objective Φ with expectations E[·] for a non-robust formulation:

$$\Phi = -\left(n_{\text{w}}(t_{\text{end}}) - E\left[n_{\text{w}}(t_0)\right]\right)^2 + 10^4 \cdot \left(n_{\text{hp}}(t_{\text{end}})\right)^2 \qquad (21)$$

$$s \;=\; T - 345\,K \;\leq\; 0\,, \quad q_{\text{f,max}} = u_{\max} = 50\,\frac{\text{ml}}{\text{min}}\,. \qquad (22)$$

In the robust case, possible variations in Φ and s are taken into account. Besides the mean production expressed by $\overline{\Phi}$ =E[Φ] its distance to the upper 2σ boundary $\Delta\Phi^{(2+)}$ is included. Hence, the feeding profile $\mathbf{U}^*$ is the result of the following optimization problem:

$$\begin{aligned} \mathbf{U}^* = \arg\min_{\mathbf{U}} & \left[\overline{\Phi}\left(\underline{x}_0, \mathbf{U}, \underline{\theta}\right) + \gamma\left(\Delta\Phi^{(2+)}\right)\right] \qquad (23) \\ \text{w.r.t.} \quad & \dot{\underline{x}} = \underline{f}(\underline{x}(t), u(t), \underline{\theta}), \qquad \underline{x}(t_0) = \underline{x}_0\,, \\ & 0 \;\leq\; t \leq 600\,\text{s} \qquad 0 \;\leq\; u(t) \leq u_{\max}\,, \\ & \overline{s}\left(\underline{x}(t)\right) \;+\; \lambda\,\Delta s^{(2+)} \;\leq\; \underline{0} \end{aligned}$$

The inequality constraint is replaced here by a robust formulation as well. Both robust process designs, 1GMD and 32GMD, must keep a 2σ safety distance to the mean value $\overline{s}$ of that constraint ($\Delta s^{(2+)}$, $\lambda = 1$) based on their individual stochastic simulation. The variation of the objective $\Delta\Phi^{(2+)}$ can then be neglected using $\gamma = 0$ since it is mainly influenced by the temperature limitation. The solution of the non-linear stochastic optimization problem (23) is calculated using the SNOPT7 algorithm (SQP) from the Tomlab® optimization toolbox for MATLAB with input constraints for $u(t)$ and nonlinear inequality constraints $s\big(\underline{x}(t)\big)$.

Fig 3 shows the stochastic simulation of the reaction temperature based on the optimization results. The probabilistic nature is indicated by the course of the mean value (solid line) and the $\pm 2\sigma$ confidence boundary (dashed line). Additionally, the experimental realizations of both robust designs are shown (left: 1GMD, right: 32GMD) using two different illustrations: In the upper plots the measured temperatures T of each process run are printed as gray lines. Due to the density of the trajectories a core estimator is used to form a probability density. The experimental densities are depicted in the center row of plot with dark areas referring to dense courses of experimental results. In the lower plots the optimal open-loop feeding profiles based on each uncertainty description are shown. When comparing the experimentally obtained temperature curves with their individual predictions a slight overestimation at high temperatures T can be observed in both cases. This results from the simplified exhaust gas description which neglects off gas due to vapor pressure. At 60 C the vapor pressure is about 200 mbar leading to a significant vapor flow at the real plant. This model defect, however, affects both robust designs in the same way, and, thus, does not interfere with the comparison.

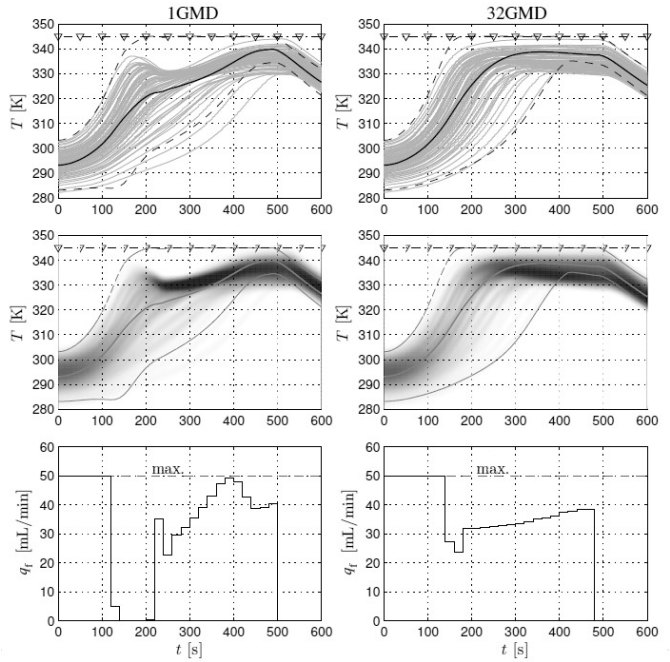

Fig. 3. Robust process designs and 72 experimental realizations, each. Left column: 1GMD design, right column: 32GMD design. The bottom row shows the optimal feeding profiles q_{f} of H_2O_2 with the maximal feed rate $q_{\text{f,max}} = 50$ mL/min indicated as dash-dotted line. In the upper plots the measured reaction temperatures of all 72 realizations are given: At the very top as plain individual gray lines. Using a core estimator these results are transferred to probability densities to illustrate densities with darker shades in the middle row. The obtained experimental results are compared with the stochastic simulation of the optimal solutions, represented by its mean value (solid lines) and $\pm 2\sigma$ boundaries (dashed lines).

Based on the results of the 1GMD design (left) the deficit of this uncertainty prediction becomes evident: The real temperature distribution with respect to the input uncertainties T_M and V_0 shows more and more skewness with the tail pointing towards lower temperatures. As it is approximated with a single normal density it overestimates the variation towards higher temperatures leading to an unnecessarily defensive process de-

sign, especially around $t = 200 - 400\,\mathrm{s}$. This limitation in the approximation of the process uncertainties can be overcome using several normal distributions. The stochastic simulation based on the 32GMD captures the asymmetrical character of the temperature uncertainty and therefore allows for a better exploitation of the temperature constraint without introducing additional risk. This results in a more offensive process design (see feed rate around $t = 100 - 200\,\mathrm{s}$), and, thus, in a 9 % higher feed and therefore in a 9 % higher productivity.

5. ROBUST PROCESS CONTROL

Closed-loop process control has been applied using stochastic online optimization (OT), i.e., the optimization always runs until the end of the batch. Based on the current state estimation a complete new robust optimal process design is calculated with respect to the objective (21). Using online optimization ensures that the control result is only determined by the different uncertainty consideration and not by a specific choice of a control and prediction horizon in a NMPC framework. Although the temperature can almost be measured continuously the measurement interval has been stretched artificially to $t_\mathrm{m} = 50\,\mathrm{s}$ to allow for a pronounced uncertainty evolution between measurement updates. This interval also corresponds to the calculation time for the state estimation $t_\mathrm{est} = 2\,\mathrm{s}$ and the online optimization $t_\mathrm{calc} = 48\,\mathrm{s}$. For the state estimation the SPKF algorithm was used [Julier et al. (2000); van der Merwe (2004)]. In order to allow for convergence of the optimization algorithm within this very time span the number of normal densities had to be reduced. Compared to the 32 densities used for the robust open-loop design the cooling temperature is now only described by 4 normal densities similar to Fig. 2. All other uncertainties, i.e., V_0 and $\underline{\theta}$, are represented by a single normal multivariate distribution. Therefore, this section compares two robust closed-loop control schemes with uncertainty description based on a 1GMD and a 4GMD, respectively.

When applying the two robust control concepts to the plant it became quickly evident that the educt concentration H_2O_2 in the storage tank had declined significantly. In order to avoid a new parameter identification the model parameter χ responsible for the uncertain educt concentration is increased. It now covers the range of 27-35 % H_2O_2 with respect to 6 standard deviations. Retaining the above identified correlation coefficients of the parameters, its covariance matrix $\mathbf{C}_{\underline{\theta}}$ is recalculated according to the new standard deviation $\sigma_\chi = 4/3\,\%$. Due to this general increase of uncertainty the robust controlled processes turn out to be more defensive compared to the robust designs from the previous section in Fig. 3. Therefore, the spread of the measured temperatures in theses experiments is rather big despite of closing the loop for the measurements.
In Fig. 4 the experimental results of the robust online optimization based on the adapted model are shown. The product distribution at the end of both robust control schemes (middle row) indicates, that the more detailed uncertainty description of the 4GMD (left column) results in a higher amount of product. Processes that are affected by the lower cooling temperatures are difficult to control at the beginning due to the input constraint $u_\mathrm{max} \leq 50\,\mathrm{mL/min}$. In later stages, the demand for low educt concentrations at the end of the process inhibits the feeding rate leading to overall quite passive process runs. This can be confirmed by looking at the estimated educt concentration (H_2O_2, first row) of both control schemes. Increasing the feeding rate would inevitably lead to a significant accumulation

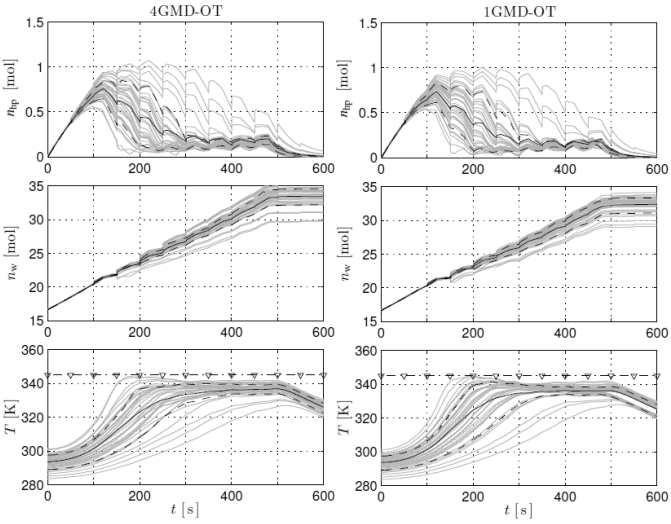

Fig. 4. 42 experimental realizations of the two robust online optimizations with adapted educt parameter χ. Left: 4GMD control scheme, right: 1GMD control scheme. For the unmeasured states n_hp and n_w the state estimations have been connected by model simulations. Reactor temperature T shows the online measurements (gray lines). In all plots the mean values (black lines) and the upper and lower 1σ confidence boundaries (dashed lines) are illustrated.

of educt. Due to the generous 6σ assumption for the uncertainty of χ the process fluctuations are being overestimated in most process phases. This results in a strong response of the current feeding rate after the first measurement is obtained. Future feeding rates, however, remain rather unaffected due to the large uncertainties that are quickly built up during the stochastic simulation. This is the reason why the curves of the mean values of all process variables are slightly oscillating. However, both robust control schemes are experiencing the same conditions, i.e., a simplified model and a generous assumption for the uncertainty of χ, such that the comparison is not biased in any way. Therefore, the control schemes can be evaluated quantitatively regarding their productivity and the result is shown in Fig. 5. The left part shows the quantity of product estimations $\hat{n}_\mathrm{w}(t_\mathrm{end})$ at the end of the process. The corresponding histogram of the 4GMD control scheme is slightly shifted towards higher product yields compared to that of the 1GMD. However, since these are only estimated values also the total volume of fed educt V_f has been illustrated in the plot on the right. Assuming that the demanded condition for low educt concentrations at the end of the process is met the total volume of feeding correlates directly with the product yield. In this graph the histogram of the 4GMD control scheme is also shifted towards higher feedings compared to the one of the 1GMD control scheme confirming the previous result. In order to allow for a quantitative evaluation of the histograms, their mean values are given in Tab. 3. Based on the total feed volume V_f the benefit of the more detailed uncertainty description can be estimated with 2.8 %. In contrast to the robust offline optimization where the more detailed stochastic simulation resulted in 9 % higher yield the benefit is comparatively small. This is not so much due to the less detailed uncertainty description (32GMD vs. 4GMD) but rather due to the frequently correcting process control which avoids the generation of larger uncertainties, and, thus, marginalizes the benefits of a detailed stochastic simulation.

OT	Expection Values	
	$\hat{n}_\mathrm{w}$	V_f
1GMD	32.41	326.35
4GMD	33.46	335.63

Table 3. Expectations of the estimated amount of product at the end of the process $\hat{n}_\mathrm{w}(t_\mathrm{ende})$ and the total volume of fed educt V_f for all 42 experimental realizations of both control schemes.

6. CONCLUSION

The 144 robust open-loop process designs and the 84 robust closed-loop control schemes have clearly shown that a more detailed uncertainty consideration leads to better process prediction in stochastic simulations. Moreover, they are able to illustrate that also the productivity can be increased when safety constraints limit the production capabilities. Generally spoken, a better knowledge about future evolutions of process uncertainties reduces over- or underestimation of such. If overestimation is being reduced, process constraints can be exploited more efficiently without increasing the already involved risk. If underestimations are being corrected, critical process phases can be avoided, and, thus, the process safety will improve. When considering a detailed uncertainty description in a robust closed-loop control scheme the advantages are partially marginalized because the measurement feedback reduces the systems uncertainties. Depending on the measurement situation the system state can be estimated more or less frequently. In general, it can be concluded that the longer a process remains unobserved the more beneficial is a detailed uncertainty description based on Gaussian mixture densities. When using chance constraint programming (CCP) [Li et al. (2008)] exact uncertainty predictions with respect to the model can be obtained and similar robust processes can be expected. In contrast to GMD based methods, however, the use of CCP does not allow for the prediction of complete probability densities whose knowledge can be further beneficial, e.g., for a more detailed state estimation.

ACKNOWLEDGEMENTS

Financial support of the first author by the Deutsche Forschungsgemeinschaft is gratefully acknowledged in the context of the center of excellence UniCat.

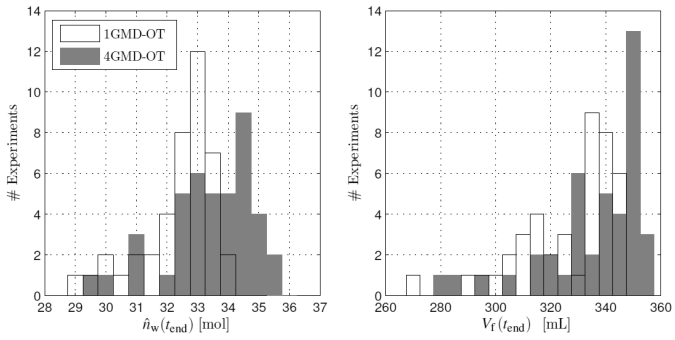

Fig. 5. Amount of product obtained from both robust online optimizations. Left: Frequency of estimated amount of product at the end of the process $\hat{n}_\mathrm{w}(t_\mathrm{end})$. Right: Frequency of the total volume of fed educt V_f.

Material constants			
Substance i	$\rho_i \left[\frac{\mathrm{g}}{\mathrm{L}}\right]$	$c_{p,i} \left[\frac{\mathrm{J}}{\mathrm{gK}}\right]$	$M_i \left[\frac{\mathrm{g}}{\mathrm{mol}}\right]$
H_2O_2 (hp)	1450	2.62	34
H_2O (w)	1000	4.18	18
O_2 (o)	–	0.92	32
PI	–	0.32	166

Table 4. Material constants: Density ρ, specific heat capacity c_p and mole mass M.

REFERENCES

Bray, W.C. and Liebhafsky, H.A. (1931). Reactions involving hydrogen peroxide, iodine and iodate ion. i. introduction. *Journal of the American Chemical Society*, 53(1), 38–44.

Dempster, A., Laird, N., and Rubin, D. (1977). Maximum likelihood from incomplete data via the em algorithmm. *Jounal of the Royal Statistical Society*, 39 Series B (Methodological), 1–38.

Efron, B. (1986). Bootstrap methods for standard errors, confidence intervals and other measures of statistical accuracy. *Statistical Science*, 1(1), 54–75.

Julier, S. and Uhlmann, J.K. (1996). A general method for approximating nonlinear transformations of probability distributions. Technical report, Dept. of Engineering Science, University of Oxford.

Julier, S., Uhlmann, J., and Durrant-Whyte, H. (2000). A new method for the nonlinear transformation of means and covariances in filters and estimators. *IEEE Transactions on Automatic Control*, 45(3), 477–482. doi:10.1109/9.847726.

Li, P., Arellano-Garcia, H., and Wozny, G. (2008). Chance constrained programming approach to process optimization under uncertainty. *Computers & Chemical Engineering*, 32(1–2), 25–45. doi:10.1016/j.compchemeng.2007.05.009.

Liebhafsky, H.A. and Mohammad, A. (1933). The kinetics of the reduction, in acid solution, of hydrogen peroxide by iodide ion. *Journal of the American Chemical Society*, 55(10), 3977–3986.

Nørgaard, M., Poulsen, N.K., and Ravn, O. (2000). New developments in state estimation for nonlinear systems. *Automatica*, 36(11), 1627–1638.

Rossner, N., Heine, T., and King, R. (2010). Quality-by-design using a gaussian mixture density approximation of biological uncertainties. In *Proc. of the 11th Computer Applications in Biotechnology (CAB)*, 7–12.

Schmitz, G. (2011). Iodine oxidation by hydrogen peroxide and Bray-Liebhafsky oscillating reaction: effect of the temperature. *Physical Chemistry Chemical Physics*, 13, 7102–7111.

Sonntag, D. (1990). Important new values of the physical constants of 1986, vapour pressure formulations based on its-90, and psychrometer formulae. *Zeitschrift fr Meteorologie*, 40(5), 340–344.

Steudel, R., Krossing, I., and Steudel, Y. (2008). *Chemie der Nichtmetalle*. De Gruyter, 3. edition.

Tørvi, H. and Hertzberg, T. (1998). Methods for evaluating uncertainties in dynamic simulation - a comparison of performance. *Computers & Chemical Engineering*, 22(1001), 985–988.

van der Merwe, R. (2004). *Sigma-Point Kalman Filters for Probabilistic Inference in Dynamic State-Space Models*. Ph.D. thesis, OGI School of Science & Engineering, Oregon Health & Science University, Portland, OR, USA.